RSC Advances

PAPER

View Article Online
View Journal | View Issue



Cite this: *RSC Adv.*, 2022, **12**, 2668

# A mitochondria targetable near-infrared fluorescence probe for glutathione visual biological detection†

Mingxuan Jia,[a] Liangnian Wei,[b] Yuxun Lu,[a] Ruqiu Zhang,[cd] Qiuling Chen,[a] Wenjiang Xia,[cd] Ye Liu,[b] Fan Li[d] and Ying Zhou *[a]

Glutathione (GSH), an abundant non-protein thiol, plays a crucial role in numerous biotic processes. Herein, a mitochondria-targeted near-infrared GSH probe (**JGP**) was synthesized, which displayed desired properties with high specificity and sensitivity, appreciable water solubility, and rapid response time. In the presence of GSH, nearly a 13-fold fluorescence emission growth appeared at 730 nm and the solvent color changed from blue to cyan. The sensing mechanism of **JGP** and GSH was confirmed by a high-resolution mass spectroscopy analysis. Moreover, good cell penetration enabled **JGP** to be successfully used for imaging biological samples such as HeLa cells, *C. elegans*, and especially rat brain slices. Imaging experiments showed that **JGP** could monitor the GSH concentration changes with a dose-dependent direct ratio in all the tested samples. The successful application of **JGP** in brain imaging indicates that **JGP** is a suitable GSH optical probe, which may have wide application value in fields of brain imaging. It also lays a theoretical and practical foundation for the further application of fluorescent probes in brain sciences.

Received 8th December 2021
Accepted 5th January 2022

DOI: 10.1039/d1ra08917j

rsc.li/rsc-advances



## 1. Introduction

Glutathione (GSH) as a ubiquitous endogenous bio-thiol, is indispensable for keeping a suitable redox balance in living cells.[1] Besides being involved in signal transduction, xenobiotic metabolism, and gene regulation, it has also been considered a biomarker of the tumor microenvironment and acute liver injury. GSH levels are also closely related to various serious diseases including Alzheimer's and Parkinson's diseases and liver diseases.[2–5] Therefore, developing an effective detection tool for qualitative and quantitative analysis of GSH *in vitro* and *in vivo* is significant and urgently needed in clinical diagnosis.[6,7]

Selectively detecting GSH from several coexisting bio-thiols (cysteine, homocysteine, selenocysteine, *etc.*) is difficult because of their analogous molecular structures and similar reactivities.[8–11] Compared with the traditional detection methods, fluorescent probes afford a variety of testing advantages such as real-time spatial and *in situ* imaging, high sensitivity, non-invasiveness, and low damage for biosamples.[12,13] In recent years, some mediocre designs of fluorescent probes for testing GSH mostly imitate the antiquated mechanism such as Michael addition,[14–17] nucleophilic substitution,[18–23] and disulfide or Se–Se bond break,[24–29] *etc.*[30,31] However, most of them have the disadvantages of slow response time or poor selectivity, and these problems remain a challenge.

Brain science has always been a compelling research field, and has become more and more popular in recent years. The content and distribution of some substances in the brain are closely related to common brain diseases.[32,33] In particular, GSH, as a reductive substance, can effectively fight against reactive oxygen species in the brain. In previous reports, hippocampal GSH levels in human postmortem brain samples have been reported to decrease with age.[34] Besides, the previous study using the MPTP mouse model of Parkinson's disease (PD) showed GSH depletion with increased oxidative stress and EAAC1 dysfunction in the midbrain.[35] All these observations indicated that the content of GSH in the brain had a potential relationship with neurodegenerative diseases such as Alzheimer's disease (AD) and PD. However, research focusing on brain GSH imaging is very limited due to the problem of poor anti-interference or unspecific selectivity.[36,37] Therefore, we believe that developing a near-infrared, highly selective GSH probe for brain imaging is of great significance.

Fluorescence imaging is a common method of biological analysing,[38,39] based on the previous works,[40] we chose the typical fluorescence mechanism of intramolecular charge

[a]College of Chemical Science and Technology, Yunnan University, Kunming 650091, P. R. China
[b]Institute of Medical Biology, Chinese Academy of Medical Sciences, Peking Union Medical College, Kunming, Yunnan 650000, P. R. China
[c]School of Basic Medical Sciences, Kunming Medical University, Kunming 650500, P. R. China
[d]Department of Pathology and Pathophysiology, Medical College, Yunnan University, Kunming 650091, P. R. China

† Electronic supplementary information (ESI) available. See DOI: 10.1039/d1ra08917j

transfer (ICT) to regulate the fluorescence switch. Meanwhile, a positive nitrogen ion was introduced into the probe to ensure the mitochondrial localization ability.[41–44] Thus, an ICT-based, 2,4-dinitrobenzenesulfonyl group modified near-infrared fluorescent probe **JGP** for the detection and bio-imaging of GSH was synthesized. As anticipated, the probe showed high specificity and sensitivity, an excellent linear relationship with the analyte, and good mitochondria colocalization ability. Moreover, stable optical properties and good penetration provided **JGP** with biological imaging capability in complex biological samples such as *C. elegans* and rat brain slices.

## 2. Results and discussion

### 2.1. Spectral responses of JGP toward GSH

First, the optical response of **JGP** toward GSH was investigated in phosphate buffer (0.02 mM, pH 7.4, PBS : EtOH = 3 : 7). As shown in Fig. 1A, **JGP** alone displayed extremely weak fluorescence. A fluorescence emission growth appeared at 730 nm after incubating **JGP** with the increasing concentration of GSH, and the solvent colour changed from blue to cyan. Free **JGP** exhibit two absorption maxima around 555 nm and 610 nm. The absorption band at 555 nm disappeared with the addition of GSH, whereas a new absorption band appeared at 715 nm (Fig. 1B), suggesting **JGP** responds to GSH.

The fluorescence intensity at 730 nm was linearly proportional to the GSH concentration in the range of 0–15 μM with a limit of detection (LOD) of $6 \times 10^{-7}$ M (Fig. 1C). Intracellular concentrations[45,46] of Cys (30 μM), Hcy (12.5 μM), GSH (1 mM), thiol-lacking amino acids (200 μM) and other analytes (10 μM) were selected as interference potential materials to test the selectivity of probe **JGP** (Fig. 1D). The probe had little response to all compounds other than GSH. Considering that sulfites are toxic to organisms and are present in very small quantities *in vivo*,[46] it can be recognized that **JGP** had an excellent selectivity towards GSH. As shown in Fig. S5,† probe **JGP** was stable between pH 2.0 to 11.0 and worked well between pH 6.6 to 10.0 in response to GSH. Therefore, **JGP** can be used in physiological conditions such as in living cells.

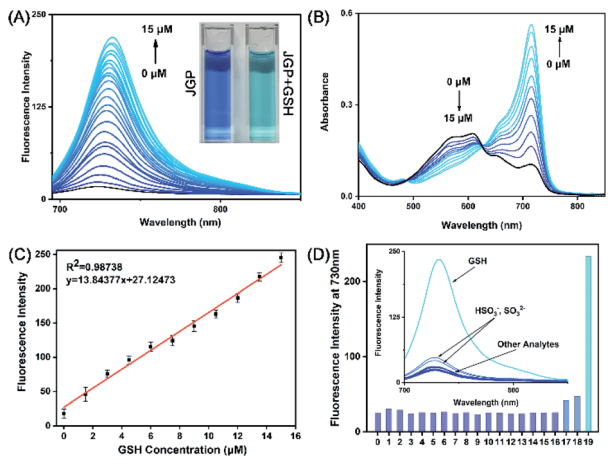


Fig. 1 (A) Fluorescence responses ($\lambda_{ex/em}$ = 680 nm/730 nm) of probe **JGP** in the presence of the increasing amount of different concentrations of GSH (0–15 μM) in the solutions. (B) UV-Vis absorption responses of probe **JGP** in the presence of increasing concentrations of GSH (0–15 μM). (C) The linear relationship between probe **JGP** and increasing concentrations of GSH (all solvent system was $CH_3CH_2$-OH : PBS, v/v = 7.3, pH = 7.4). The detection limit (LOD) was calculated to be 0.6 μM based on the expression $3S/K$. (D) Fluorescence responses ($\lambda_{ex/em}$ = 680 nm/730 nm) of probe **JGP** with the addition of various substances ((0) blank, (1) Cys (30 μM), (2) Hcy (12.5 μM), (3) Leu, (4) Ser, (5) Val, (6) Pro, (7) Glu, (8) $H_2O_2$, (9) $H_2S$, (10) $NO_3^-$, (11) $ClO^-$, (12) $Ni^{2+}$, (13) $Cr^{3+}$, (14) $Fe^{3+}$, (15) $HSO_4^-$, (16) $SO_4^{2-}$, (17) $HSO_3^-$, (18) $SO_3^{2-}$, (19) GSH (1 mM)). **JGP** concentration: 20 μM.

### 2.2. Study of mechanism

ESI-MS was carried out to verify the reaction mechanism, as demonstrated in Fig. S3.† After the reaction of **JGP** with GSH, a new peak at *m*/*z* 448.2303 was assigned to the product of compound **4** ($[M]^+$ calcd 448.2271) formed after the bond breaking reaction between **JGP** and GSH. It indicates that the response mechanism of **JGP** to GSH is based on the removal of 2,4-nitrobenzene sulfonate and **JGP** could be used for GSH detection as a fluorescent probe.

### 2.3. Cell labeling and intracellular colocalization studies

According to the cytotoxicity study (Fig. S6†), the inhibitory rate of the probe **JGP** on normal cells was much lower than that on tumor cells at the same concentration. In order to further verify the detection capability of **JGP** for GSH in cells, fluorescence imaging studies were carried out using HeLa cells, in the presence of NEM (*N*-ethylmaleimide) to get rid of GSH in some bio-samples. The acquired fluorescence images revealed that the fluorescence intensity in the untreated HeLa cells (Fig. 2Aa3) was greater than that in NEM-treated cells (Fig. 2Ab3). The fluorescence imaging results showed in Fig. 2B demonstrated that **JGP** could monitor the GSH concentration changes in a dose-dependent manner.

Further, we explored the intracellular localization ability of **JGP** in HeLa cells using commercial mitochondria-specific tracker-Mito Tracker Green. The extent of fluorescence overlap for **JGP** with mitochondria was codified in the form of the Pearson's overlap coefficient (PC) of 0.94, an average over at least 3 independent experiments (Fig. 3). As anticipated, the presence of the positive ion on nitrogen in the probe **JGP** afforded an excellent ability for staining mitochondria. Therefore, probe **JGP** can be potentially applied to analyse exogenous/endogenous GSH content *in vivo* qualitatively.

### 2.4. Confocal imaging of *C. elegans* and rats brain slices

In order to further validate the imaging ability of **JGP** in more sophisticated biological samples, the *in vivo* imaging of glutathione was evaluated in *C. elegans* and rat brain slices. *C. elegans* were randomly divided into four groups: the first group was blank; the second group was only treated with probe **JGP** (20 μM); the third group was first treated with NEM (20 μM) to get rid of the endogenous GSH and then incubated with probe **JGP** (20 μM); the last group was incubated with NEM, **JGP**, and GSH in turn. As evident from Fig. 4A and C, there was almost no fluorescence response from the blank group. In group 2 and

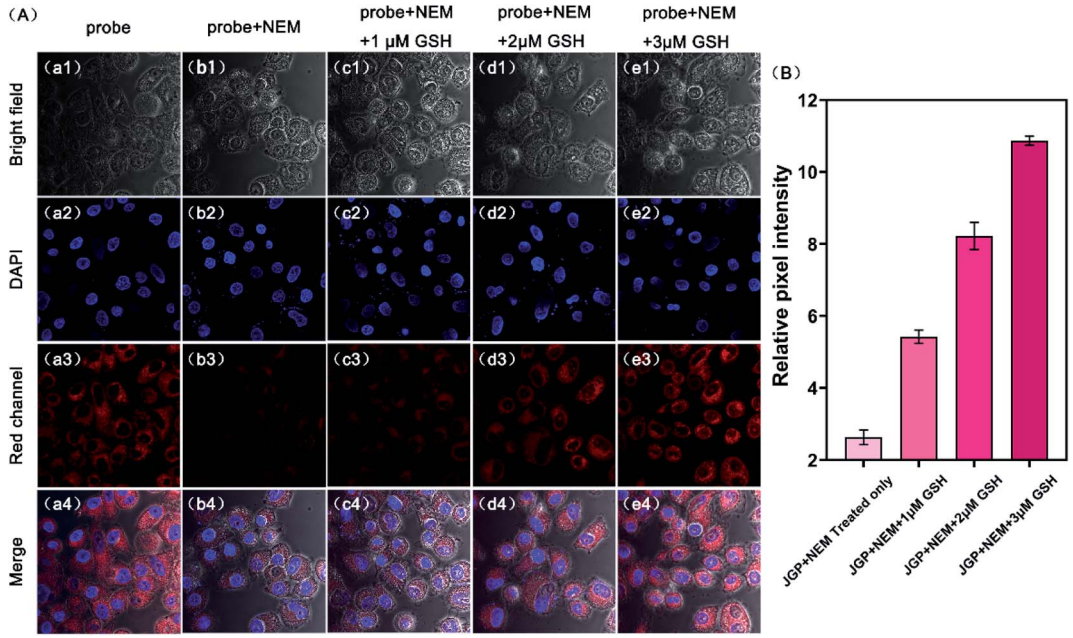


Fig. 2 (A) Confocal fluorescence images of HeLa cells. (a1)–(a4) The cells were incubated with probe **JGP** for 1 h only. (b1)–(b4) The cells were incubated with NEM (50 μM) for 30 min and then treated with probe **JGP** for 1 h. (c1)–(e4) The cells were incubated with NEM (50 μM) for 30 min, treated with probe **JGP** for 1 h, and further treated with GSH ((c1–c4) 1 μM, (d1–d4) 2 μM, (e1–e4) 3 μM) for 1 h. (B) Relative pixel intensity of red channels of HeLa cells. Objective lens: 10×; scale bar: 20 μm; incubation temperature of HeLa cells: 37 °C; **JGP** concentration: 5 μM.

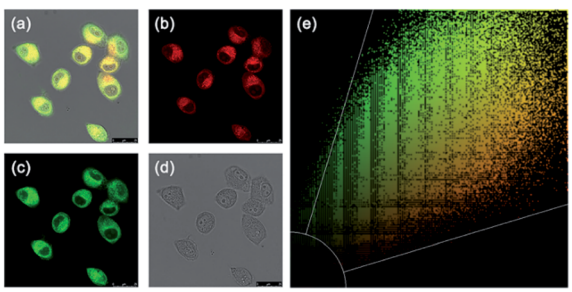


Fig. 3 HeLa cells were incubated with **JGP** (5 μM) for 30 min, then incubated with Mito Tracker Green (0.4 μM) for 30 min. (a) The red fluorescence image of **JGP**, red channel = 650–750 nm. (b) The green fluorescence image of Mito Tracker Green, green channel = 520–620 nm. (c) Bright field image. (d) Merged images of (a)–(c). (e) Colocalization coefficient of **JGP** and Mito Tracker Green was calculated to be 0.94.

group 4, significant fluorescence could be observed, indicating the presence of GSH in nematodes. The fluorescent intensity in group 4 was higher than that in group 2, which indicated that the concentration of GSH in nematodes increased after exogenous treatment (Fig. 4C). In third group, fluorescence intensity was significantly lower as compared to group 2 and group 4, which confirmed that NEM removed endogenous GSH in *C. elegans*. We further investigated the imaging ability of **JGP** in rat brain slices. In previous studies,[47–50] it was found that the content of GSH in the brain environment contributed to the balance of the content of reactive oxygen species (ROS) partly.

The insufficient content of GSH can interrupt the brain REDOX balance and result in the risk of stroke diseases. If the probe **JGP** can successfully image GSH in rat brain slices, it will have the possibility to monitor the changes of GSH in the brain, which is of great significance for the detection of various diseases caused by the decrease of GSH content. Frozen brain slices were chosen for confocal imaging and divided into four groups: blank group, endogenous GSH group, NEM-preincubated group (since NEM is a GSH scavenger, the lower fluorescence intensity of NEM group than that of the exogenous group would indicate that the probe **JGP** can detect exogenous GSH), and exogenous GSH group. As exhibited in Fig. 4B and D, we found that the fluorescence intensity values of the endogenous GSH group and exogenous GSH group were much higher than that of the other two groups, which directly demonstrated that the ability of probe **JGP** to image GSH in the brain environment and its potential for imaging GSH in other complex biological models. Due to the advantage of near-infrared fluorescence emission of the probe **JGP**, even the rat brain slices showed strong green autofluorescence in the confocal experiments, the bio-imaging by **JGP** can still clearly chase the GSH concentrate changes in the biological samples without any interference. Thus, **JGP** was proved to be a unique probe that can be used for monitoring and visualizing the GSH fluctuation in the internal environment of complex biological samples.

## 3. Experimental

### 3.1. Materials and instruments

All solvents and reagents were purchased commercially and used without further purification. Flash column chromatography was performed using silica gel (200–300 mesh). Mass

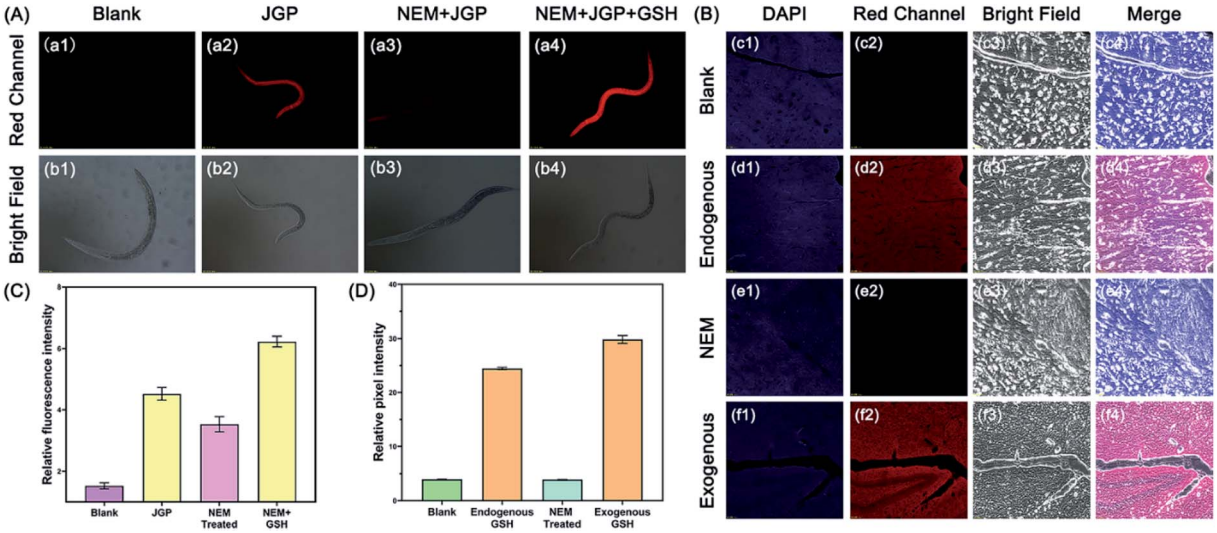


Fig. 4 (A) CLSM imaging of *C. elegans* (N2). (a1) and (b1) Blank. (a2) and (b2) *C. elegans* were incubated with probe **JGP** for 2 h. (a3) and (b3) *C. elegans* were first incubated with NEM for 30 min before incubated with probe **JGP**. (a4) and (b4) *C. elegans* were first incubated with NEM for 30 min. Next, *C. elegans* were treated with probe **JGP** for 2 h and further treated with GSH (400 μM) for 2 h. (B) Confocal imaging of rat brain slices. (c1)–(c4) Blank. (d1)–(d4) The brain slices were treated with probe **JGP** for 1 h. (e1)–(e4) The brain slices were first incubated with NEM for 15 min before incubated with probe **JGP**. (f1)–(f4) The brain slices were first incubated with NEM for 30 min. Next, brain slices were treated with probe **JGP** for 1 h, and further treated with GSH (50 μM) for 1 h. (C) Relative pixel intensity of red channels of *C. elegans*. (D) Relative pixel intensity of red channels of rat brain slices. Objective lens: 10×; incubation temperature of *C. elegans*: 20 °C; incubation temperature of brain slices: 37 °C. **JGP** concentration: 20 μM, NEM concentration: 500 mM.

spectra were recorded on cation SpecHiResESI mass spectrometer. NMR spectra were recorded on a 400 MHz spectrometer (Bruker, Germany).

### 3.2. Design and synthesis of probe JGP

Cyanine derivative was selected as the fluorophore due to its excellent photophysical properties, and the positively charged moiety of indole ammonium cation was chosen for mitochondria targeting. 2,4-Dinitrobenzenesulfonyl group was introduced at the hydroxyl site of the fluorophore as both a GSH responsive group and a quencher. Synthesis methods of compounds **1**, **2**, **3**, and **4** are according to the previous literature.[51] The synthetic route of **JGP** is illustrated in Scheme 1, and it was characterized and confirmed by $^{1}$H NMR and $^{13}$C NMR spectroscopy (Fig. S1†). To synthesize **JGP**, compound **4** (287.75 mg, 0.5 mmol) was dissolved in anhydrous dichloromethane. To this, triethylamine (0.10 mL, 0.75 mmol) and 2,4-dinitrobenzenesulfonyl chloride (265.94 mg, 1 mmol) were added, and the mixture was reacted at room temperature for 3 hours. After completion of the reaction, the resulting solution was extracted with deionized water three times (3 × 20 mL). The organic layer was dried over $Na_2SO_4$, and then the solvent was

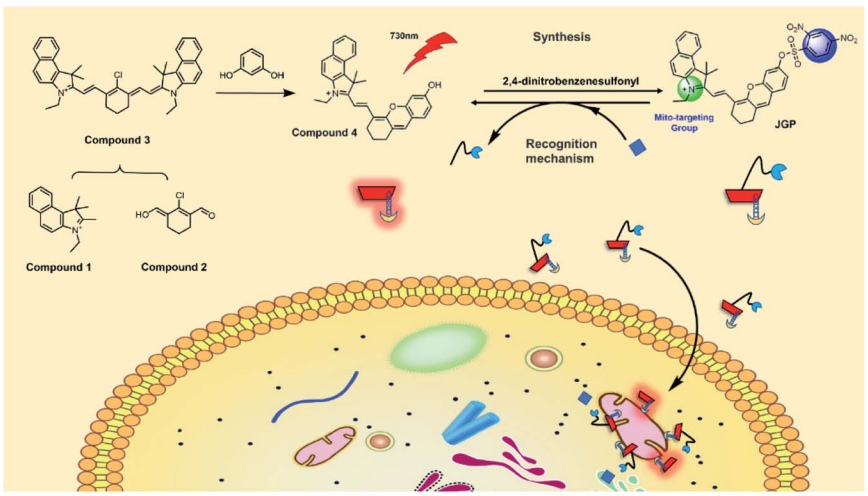


Scheme 1 Synthesis and recognition mechanism of probe **JGP**.

evaporated. The crude solid was purified by silica gel column chromatography with methanol/dichloromethane (1 : 100, v/v) to afford a cyan powder of **JGP**. Yield: 42% (169.07 mg). $^1$H NMR (400 MHz, $CDCl_3$) $\delta$ (ppm) 8.886 (d, $J$ = 2.8 Hz, 1H), 8.537 (m, 1H), 8.198 (d, $J$ = 8.4 Hz, 1H), 8.049 (m, 2H), 7.677 (t, $J$ = 7 Hz, 2H), 7.654 (m, 1H), 7.511 (t, 1H), 7.370 (m, 1H), 6.968 (m, 1H), 6.791 (m, 1H), 6.766 (m, 1H), 4.819 (q, $J$ = 6.4 Hz, 2H), 2.8885 (m, 2H), 2.762 (m, 2H), 2.076 (s, 6H), 1.972 (m, 2H), 1.639 (t, $J$ = 1.2 Hz, 3H). $^{13}$C NMR (100 MHz, $CDCl_3$) $\delta$ (ppm) 197.80, 158.18, 152.98, 151.12, 149.47, 148.83, 148.23, 147.43, 145.42, 138.23, 137.08, 134.36, 133.12, 131.83, 131.56, 130.21, 128.76, 128.45, 127.39, 126.86, 125.19, 122.65, 121.69, 120.46, 118.18, 115.52, 111.65, 110.09, 106.44, 53.05, 42.01, 29.51, 27.54, 27.43, 24.12, 20.11, 13.39. HEMS (ESI): calcd for $C_{37}H_{32}N_3O_8S^+$ $[M]^+$ = 678.1905, found $m/z$ 678.1902.

### 3.3. UV-Vis and fluorescence spectroscopy

UV-240IPC spectrophotometer (Shimadzu) and F97XP spectrofluorometer were used for acquiring the absorption spectra and fluorescence spectra, respectively, using 1 cm standard quartz cell. The emission spectrum was recorded at the excitation wavelength of 680 nm, and the excitation spectrum as monitored at the wavelength of 730 nm. The stock solution of probe **JGP** (5 mM) was prepared in ethanol.

### 3.4. Determination of the detection limit

The lowest detection limit was estimated by following regression equation as adopted in previous report.[52]

### 3.5. Cell imaging experiment and colocalization study

The HeLa cells were provided by the Kunming Institute of Zoology, Chinese Academy of Sciences. First, the cells were washed three times with PBS buffer (0.01 M, pH 7.4). After washing the cell culture dish twice with PBS buffer, HeLa cells were transferred, and 1 mL of PBS buffer was added. Next, the HeLa cells were incubated with probe **JGP** (5 μM) for 1 h, treated with a large amount of NEM (glutathione scavenger, 500 μM), followed by the addition of GSH. The Olympus laser confocal microscope (FV10i) was used to test the red channel. In the cell colocalization study, after incubation with probe **JGP** (5 μM) for 30 min, group 1 were washed twice with PBS buffer and then incubated with DAPI for 15–30 min. Then cells were then washed twice with PBS buffer and incubated with mitochondrial dye (Mito Tracker Green (10 nM)) for 30 min. The red channel (670–760 nm) fluorescence was again detected using Olympus laser confocal microscope (FV10i). Channel selection: DAPI ($\lambda_{em}$ = 461 nm); green ($\lambda_{em}$ = 500–580 nm); red ($\lambda_{em}$ = 670–760 nm).

### 3.6. *C. elegans* fluorescence imaging

*C. elegans* were divided into four groups for CLSM. The first group was the blank group. The second group was incubated with 4% formaldehyde for 30 min and then treated with **JGP** for 2 h after washing with de-aerated M9 buffer three times. The third group was incubated in de-aerated M9 buffer with NEM (1.0 mM) at 20 °C for 1 h, and then treated with GSH (200 μM) for 2 h. After fixing with 4% formaldehyde for 30 min, *C. elegans* were finally stained with 20 μM of **JGP** for 2 h. Analogously, the last group was incubated in de-aerated M9 buffer with NEM (1.0 mM) for 30 min but without GSH treatment. After the same process, the nematodes were stained with 20 μM of **JGP** for 2 h. *C. elegans* were washed with de-aerated M9 buffer three times before each step. Finally, fluorescence imaging was performed by the Olympus BX51 fluorescence microscopy.

### 3.7. Rat brain slices confocal imaging

All animal studies were approved by the Committee on Animal Research and Ethics of Yunnan University (yuncare20200353). We chose 9–11 day old C57BL/6J mice after birth. Rats were deeply anesthetized by intraperitoneal injection of 10% chloral hydrate (0.3 mL/100 g, IP). Brain tissues of the rat were taken out and then immersed in 2% paraformaldehyde solution for fixation overnight at 4 °C. After fixation, the brain tissues were transferred into 15% and 30% sucrose solution for dehydration. The mice brain tissues were frozen in liquid nitrogen with an embedding agent and then stored in a refrigerator at −20 °C. Frozen rat brain sections were prepared by the frozen section mechanism with a thickness of 20 μm. These slices were divided into 4 groups, which were incubated successively with 4,6-diamidino-2-phenylindole (DAPI) (all groups) for 30 min, 1 mM *N*-ethylmaleimide (NEM) (group 3, in PBS buffer) for 30 min, 20 μM **JGP** (group 2, 3 and 4, in PBS buffer) for 1 h, and 20 μM GSH (group 4, in PBS buffer) for 1 h. All incubation processes were carried out at 37 °C, and samples were washed thrice with red channel PBS buffer at the end of each treatment. After mounting with glycerol gelatin aqueous slide mounting medium, brain slices were transferred to Olympus laser confocal microscope (FV10i) for observation. Channel selection: DAPI ($\lambda_{em}$ = 461 nm); red ($\lambda_{em}$ = 670–760 nm).

## 4. Conclusions

We have designed and synthesized a near-infrared probe **JGP** for detecting GSH in biologic samples. The optical properties of the probe showed that it had obvious colorimetric change, fast response, excellent selectivity, good linearity with the analyte, and a low detection limit (600 nM). The probe **JGP** showed excellent cell penetration and successfully detected exogenous and endogenous GSH in HeLa cells, *C. elegans*, and the rat brain slices, with noticeable fluorescence changes. Therefore, we believe that this newly developed probe **JGP** may have potential in a wide range of applications in monitoring GSH content changes in brain science-related research and clinical medicine.

## Ethical statement

All animal procedures were performed in accordance with the Guidelines for Care and Use of Laboratory Animals of Yunnan University and approved by the Committee on Animal Research and Ethics of Yunnan University (yuncare20200353).

## Author contributions

Mingxuan Jia: investigation, probe synthesis, spectral testing and biological imaging, data curation, writing – original draft. Liangnian Wei: cell imaging test. Yuxun Lu: optical studies, brain slices imaging test. Ruqiu Zhang: brain slices imaging test. Qiuling Chen: conceptualization, optical studies. Wenjing Xia: brain slices imaging test. Ye Liu: supervision of cell imaging test. Fan Li: funding acquisition, supervision of brain slices imaging test. Ying Zhou: funding acquisition, supervision, writing and revising manuscript.

## Conflicts of interest

There are no conflicts to declare.

## Acknowledgements

This work is supported by the National Natural Science Foundation of China (22067019, 82171430) and the Scientific Research Foundation Project of Yunnan Provincial Department of Education (2021Y031). Authors thank Advanced Analysis and Measurement Center of Yunnan University for the sample testing service.

## References

1 C. Wang, X. Xia, J. Luo and Y. Qian, *Dyes Pigm.*, 2018, **152**, 85–92.
2 K. Umezawa, M. Yoshida, M. Kamiya, T. Yamasoba and Y. Urano, *Nat. Chem.*, 2017, **9**, 279–286.
3 J. Huang, Y. Chen, J. Qi, X. Zhou, L. Niu, Z. Yan, J. Wang and G. Zhao, *Spectrochim. Acta, Part A*, 2018, **201**, 105–111.
4 X. Yang, W. Liu, J. Tang, P. Li, H. Weng, Y. Ye, M. Xian, B. Tang and Y. Zhao, *Sci. Rev. Chem. Commun.*, 2018, **54**, 11387–11390.
5 N. Zhou, F. Huo, Y. Yue, K. Ma and C. Yin, *Chin. Chem. Lett.*, 2020, **31**, 2970–2974.
6 E. Camera and M. Picardo, *J. Chromatogr. B: Anal. Technol. Biomed. Life Sci.*, 2002, **781**, 181–206.
7 D. Spector, J. Labarre and M. B. Toledano, *J. Biol. Chem.*, 2001, **276**, 7011–7016.
8 D. Yue, M. Wang, F. Deng, W. Yin, H. Zhao, X. Zhao and Z. Xu, *Chin. Chem. Lett.*, 2018, **29**, 648–656.
9 W. Liu, J. Chen and Z. Xu, *Coord. Chem. Rev.*, 2021, **429**, 213638.
10 S. Lee, J. Li, X. Zhou, J. Yin and J. Yoon, *Coord. Chem. Rev.*, 2018, **366**, 29–68.
11 K. Yin, F. Yu, W. Zhang and L. Chen, *Biosens. Bioelectron.*, 2015, **74**, 156–164.
12 F. Deng and Z. Xu, *Chin. Chem. Lett.*, 2019, **30**, 1667–1681.
13 Z. Zhang, F. Wang and X. Chen, *Chin. Chem. Lett.*, 2019, **30**, 1745–1757.
14 J. Liu, Y. Sun, Y. Huo and H. Zhang, *J. Am. Chem. Soc.*, 2014, **136**, 574–577.
15 J. Chen, X. Jiang, C. Zhang, K. R. MacKenzie, F. Stossi, T. Palzkill, M. C. Wang and J. Wang, *ACS Sens.*, 2017, **2**, 1257–1261.
16 Z. Liu, X. Zhou, Y. Miao, Y. Hu, N. Kwon, X. Wu and J. Yoon, *Angew. Chem., Int. Ed.*, 2017, **56**, 5812–5816.
17 X. Zhang, L. Zhang, X. Wang, X. Han, Y. Huang, B. Li and L. Chen, *J. Hazard. Mater.*, 2021, **419**, 126476.
18 X. Xia, Y. Qian and B. Shen, *J. Mater. Chem. B*, 2018, **6**, 3023–3029.
19 J. Liu, M. Liu, H. Zhang, X. Wei, J. Wang, M. Xian and W. Guo, *Chem. Sci.*, 2019, **10**, 10065–10071.
20 J. Gao, Y. Tao, N. Wang, J. He, J. Zhang and W. Zhao, *Spectrochim. Acta, Part A*, 2018, **203**, 77–84.
21 J. Liu, Y. Sun, H. Zhang, Y. Huo, Y. Shi and W. Guo, *Chem. Sci.*, 2014, **5**, 3183–3188.
22 J. Xu, J. Pan, Y. Zhang, J. Liu, L. Zeng and X. Liu, *Sens. Actuators, B*, 2017, **238**, 58–65.
23 Z. Xu, M. Zhang, Y. Xu, S. H. Liu, L. Zeng, H. Chen and J. Yin, *Sens. Actuators, B*, 2019, **290**, 676–683.
24 F. Wang, L. Zhou, C. Zhao, R. Wang, Q. Fei, S. Luo, Z. Guo, H. Tian and W. Zhu, *Chem. Sci.*, 2015, **6**, 2584–2589.
25 F. Kong, Z. Liang, D. Luan, X. Liu, K. Xu and B. Tang, *Anal. Chem.*, 2016, **88**, 6450–6456.
26 M. Gangopadhyay, R. Mengji, A. Paul, Y. Venkatesh, V. Vangala, A. Jana and N. D. P. Singh, *Chem. Commun.*, 2017, **53**, 9109–9112.
27 Y. Liu, S. Zhu, K. Gu, Z. Guo, X. Huang, M. Wang, H. M. Amin, W. Zhu and P. Shi, *ACS Appl. Mater. Interfaces*, 2017, **9**, 29496–29504.
28 X. Zhang, Y. Huang, X. Han, Y. Wang, L. Zhang and L. Chen, *Anal. Chem.*, 2019, **91**, 14728–14736.
29 Y. Huang, Q. Liu, Y. Wang, N. He, R. Zhao, J. Choo and L. Chen, *Nanoscale*, 2019, **11**, 12220–12229.
30 X. Li, Y. Hou, X. Meng, C. Ge, H. Ma, J. Li and J. Fang, *Angew. Chem., Int. Ed.*, 2018, **57**, 6141–6145.
31 F. Wu, H. Wang, J. Xu, H. Yuan, L. Zeng and G. Bao, *Sens. Actuators, B*, 2018, **254**, 21–29.
32 J. N. Cobley, M. L. Fiorello and D. M. Bailey, *Redox Biol.*, 2018, **15**, 490–503.
33 W. Chen, Y. Guo, W. Yang, P. Zheng, J. Zeng and W. Tong, *Restor. Neurol. Neurosci.*, 2017, **35**, 217–224.
34 C. Venkateshappa, G. Harish, A. Mahadevan, M. M. S. Bharath and S. K. Shankar, *Neurochem. Res.*, 2012, **37**, 1601–1614.
35 K. Aoyama, N. Matsumura, M. Watabe and T. Nakaki, *Eur. J. Neurosci.*, 2008, **27**, 20–30.
36 D. Zhang, W. Du, B. Peng, Y. Ni, H. Fang, X. Qiu, G. Zhang, Q. Wu, C. Yu, L. Lin and W. Huang, *Sens. Actuators, B*, 2020, **323**, 128673.
37 G. Yin, Y. Gan, H. Jiang, T. Yu, M. Liu, Y. Zhang, H. Li, P. Yin and S. Yao, *Anal. Chem.*, 2021, **93**, 9878–9886.
38 H. Han, H. Tian Jr, Y. Zang, A. C. Sedgwick, J. Li, J. Sessler, X. He and T. D. James, *Chem. Soc. Rev.*, 2021, **50**, 9391–9429.
39 S. K. Pramanik and A. Das, *Chem. Commun.*, 2021, **57**, 12058–12073.
40 C.-S. Jiang, Z.-Q. Cheng, Y.-X. Ge, J.-L. Song, J. Zhang and H. Zhang, *Anal. Methods*, 2019, **11**, 3736–3740.

41 H. Xiao, Y. Dong, J. Zhou, Z. Zhou, X. Wu, R. Wang, Z. Miao, Y. Liu and S. Zhuo, *Analyst*, 2019, **10**, 653–660.
42 Z. Xu, X. Huang, X. Han, D. Wu, B. Zhang, Y. Tan, M. Cao, S. H. Liu, J. Yin and J. Yoon, *Chem*, 2018, **4**, 1609–1628.
43 X. Zhang, N. He, Y. Huang, F. Yu, B. Li, C. Lv and L. Chen, *Sens. Actuators, B*, 2019, **282**, 69–77.
44 M. Gao, F. Yu, H. Chen and L. Chen, *Anal. Chem.*, 2015, **87**, 3631–3638.
45 C. Huang and Y. Qian, *Spectrochim. Acta, Part A*, 2019, **217**, 68–76.
46 D. Shukla, P. K. Mandal, L. Ersland, E. R. Grüner, M. Tripathi, P. Raghunathan, A. Sharma, G. R. Chithya, K. Punjabi and C. Splaine, *J. Alzheimer's Dis.*, 2018, **66**, 517–532.
47 C. D. Rae and S. R. Williams, *Anal. Biochem.*, 2017, **529**, 127–143.
48 S.-J. Li, D.-Y. Zhou, Y.-F. Li, B. Yang, J. Ou-Yang, J. Jie, J. Liu and C.-Y. Li, *Talanta*, 2018, **188**, 691–700.
49 J. Xu, Y. Zhang, H. Yu, X. Gao and S. Shao, *Anal. Chem.*, 2016, **88**, 1455–1461.
50 L.-J. Zhang, Z.-Y. Wang, X.-J. Cao, J.-T. Liu and B.-X. Zhao, *Sens. Actuators, B*, 2016, **236**, 741–748.
51 A. Slivka, M. B. Spina and G. Cohen, *Neurosci. Lett.*, 1987, **74**, 112–118.
52 C. Venkateshappa, G. Harish, A. Mahadevan, M. M. S. Bharath and S. K. Shankar, *Neurochem. Res.*, 2012, **37**, 1601–1614.